Applied Catalysis B: Environmental 125 (2012) 189–196

Contents lists available at SciVerse ScienceDirect

Applied Catalysis B: Environmental

journal homepage: www.elsevier.com/locate/apcatb

CO oxidation over graphene supported palladium catalyst

Yingzhi Li [a], Yue Yu [a], Jian-Guo Wang [b,*], Jie Song [c], Qiang Li [c], Mingdong Dong [c], Chang-Jun Liu [a,**]

[a] Advanced Nanotechnology Center, School of Chemical Engineering and Technology, Tianjin University, Tianjin 300072, China
[b] College of Chemical Engineering and Materials Science, Zhejiang University of Technology, Hangzhou, Zhejiang 310032, China
[c] Interdisciplinary Nanoscience Center (iNANO) and Department of Physics and Astronomy, Aarhus University, DK-8000 Aarhus C, Denmark

ARTICLE INFO

Article history:
Received 25 December 2011
Received in revised form 19 April 2012
Accepted 21 May 2012
Available online 29 May 2012

Keywords:
Catalyst
CO oxidation
DFT
Graphene
Palladium

ABSTRACT

Graphene supported palladium (Pd) catalyst has been prepared using the conventional impregnation and hydrogen reduction method. Highly dispersed nano particles are formed on the support graphene. The density functional theory (DFT) study and the catalyst characterization using Raman and X-ray photoelectron spectroscopy confirm that the oxygen containing groups play an important role in stabilizing Pd clusters on graphene. The first layer of the metal particle mainly presents as PdO_x. The graphene supported Pd catalyst shows superior catalytic activity and high stability for CO oxidation. The kinetic studies indicate that CO oxidation over the graphene supported Pd catalyst follows the Langmuir–Hinshelwood (L–H) mechanism.

1. Introduction

Graphene has attracted an increasing attention as a zero bandgap, sp^2-hybridized carbon material. It is promising for many applications, like molecular electronics, sensors, energy production, energy conversion and storage, because of its extraordinary thermal, mechanical, optical and electrochemical properties [1]. Two-dimensional (2D) sheet of graphene also possesses an extremely high surface-to-volume ratio, presenting interesting 2D support structures for catalytic reactions [2]. In addition, due to the inevitable carbon-vacancy defect and the functional groups presented in chemical derived graphene, metal ions can be adsorbed and intercalated into graphene sheets to form thermal stable composite materials [2]. On the basis of its unique properties, graphene is expected to be an excellent supporting material for various heterogeneous catalysts [3,4].

Various strategies have been developed for the synthesis of metal or metal oxide-embedded graphene composites, including chemical method [5], photo-synthesis [6] and microwave assisted synthesis [7,8]. Several studies have been addressed the applications of graphene for various catalytic reactions. Most of the reported graphene based catalysts reveal high activity and stability [3,4,9–11]. However, few studies [12] have been conducted to use the graphene or graphene supported catalyst for the gas–solid catalytic reaction, like CO oxidation, although numerous potential applications exist. Actually, CO oxidation is of great significance in fundamental studies as the simplest model catalytic reaction. It is one of the most important reactions, which is applicable to emission control or to the removal of trace amount of CO for fuel cell application [13–15].

In the theoretical research, several studies have shown that graphene based catalysts possess a good activity for CO oxidation. Some studies [2] have demonstrated that the catalytic activity can be influenced by the carbon-vacancy defect in graphene, the partially occupied *d* orbital localized in the vicinity of the Fermi level, the electronic structures of the metal clusters and the strong interaction between the metal clusters and graphene. However, the oxygen functional groups have not been taken into account, which is highly stable on the chemical derived graphene, and is likely to have an effect on the catalyst structure and catalytic activity. Some other calculations illustrated that the vacancies or the edges in graphene are also able to catalyze the CO oxidation [16].

In this study, a simple, low-cost, high-efficient hydrogen reduction method was employed to synthesize highly dispersed palladium (Pd) nanoparticles on graphene sheets. By the combination of catalyst characterization and DFT study, the interaction between Pd nanoparticles and graphene have been investigated, which is also useful for understanding the interaction between Pd nanoparticles and reduced graphene oxide. The properties of the graphene supported Pd catalyst were evaluated by CO oxidation. The kinetic studies have also been conducted.

* Corresponding author. Tel.: +86 571 88871037.
** Corresponding author. Tel.: +86 22 27406490; fax: +86 22 27406490.
E-mail addresses: jgw@zjut.edu.cn (J.-G. Wang), ughg_cjl@yahoo.com (C.-J. Liu).

0926-3373/$ – see front matter © 2012 Elsevier B.V. All rights reserved.
http://dx.doi.org/10.1016/j.apcatb.2012.05.023

2. Experimental

2.1. Preparation of the graphene supported Pd catalyst

Graphene in this work was synthesized according to the Hummers method [17] and thermal reduction [18]. Briefly, the graphite powder (2 g, 325 mesh, Alfa Aesar) was pre-oxidized in a solution of concentrated H_2SO_4 (15 mL), $K_2S_2O_8$ (2.5 g), and P_2O_5 (2.5 g). The solution was kept at 80 °C for about 6 h. And then it was cooled to room temperature and diluted with 500 mL deionized water (DI). The mixture was filtered, washed and dried to obtained pre-oxidized graphite. The pre-oxidized graphite was re-oxidized by putting into 0 °C concentrated H_2SO_4 (150 mL) with gradual addition of $KMnO_4$ (25 g) under stirring and ice-cooling. The mixture was kept at 35 °C for 4 h. After that, it was diluted gradually in an ice-bath-cooled environment with 600 mL DI water, followed by addition of 30 mL H_2O_2. The acquired brilliant yellow solution was filtered and washed with 1:10 HCl aqueous solution (1 L) and DI water (1 L), dialyzed for one week and then dried at 35 °C in a vacuum drier for 2 days. The dried graphite oxide powder was thermally reduced and exfoliated into individual graphene sheets with a rapid heating to 1050 °C for 0.5 min in a quartz tube purging with pure argon.

Incipient wetness impregnation was employed to prepare the graphene supported Pd catalyst. A solution of tetrachloropalladinic acid (H_2PdCl_4) was prepared by adding different amount of $PdCl_2$ (Tianjin Delan Fine Chemical Plant, China; 99% in purity) into HCl aqueous solution (2 M) under stirring and heating until complete dissolution. The graphene powder was then impregnated with the H_2PdCl_4 solution for 10 h at room temperature, followed by drying at 110 °C for another 10 h. The Pd loading amount is 2 wt%, 6 wt% and 10 wt%.

2.2. Characterization of the catalysts

X-ray diffraction (XRD) patterns were measured on a Rigaku D/MAX-2500 V/PC using Cu Kα radiation (λ = 0.154056 nm) at 40 kV and 200 mA. The wide-angle XRD patterns were collected at a scanning speed of 4°/min over the 2θ range of 5–90°. High resolution transmission electron microscopy (TEM) images were recorded with a Philips Tecnai G^2 F20 operated at 200 kV. The reduced catalyst was dispersed and dropped on the carbon-coated copper grids after sonication for 30 min. X-ray photoelectron spectroscopy (XPS) analyses were performed on a PerkinElmer PHI-1600 spectrometer with Mg Kα (1253.6 eV) radiation. Raman spectra were obtained with a DXR Raman microscope configuring with a 532 nm wavelength laser and a full-range grating. All measurements were accomplished under ambient condition.

2.3. CO oxidation

CO oxidation was carried out in a fixed-bed quartz-tube reactor (with an inner diameter of 4 mm) under ambient pressure. Before the reaction, the H_2PdCl_4/graphene sample obtained in Section 2.1 (10 mg, for each test) was packed in the tube. The sample was then heated to 300 °C (10 °C min^{-1}) in the flowing argon (20 mL min^{-1}) and reduced by a flowing mixture of H_2 and argon (5% H_2; 20 mL min^{-1}) at 300 °C for 2 h. Subsequently, the sample was cooled to 40 °C in flowing argon. CO oxidation was initiated. The gaseous mixture of CO, O_2 and N_2 (volume ratio 1:20:79; 20 mL min^{-1}) was introduced into the reactor, corresponding to a gas hourly space velocity (GHSV) of 120,000 mL h^{-1} (g cat)$^{-1}$. The gas effluent was analyzed online by a gas chromatograph (Agilent 6890D) equipped with a 2-m TDX-01 packed column and a thermal conductivity detector (TCD), using argon as the carrier gas. For the convenience of the discussions, the graphene supported Pd catalyst by hydrogen reduction is assigned as Pd-GE.

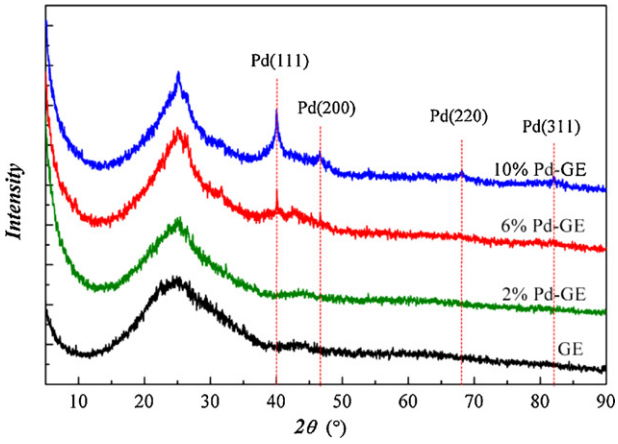

Fig. 1. XRD patterns of graphene and Pd-GE.

2.4. DFT study

All calculations have been carried out under the PW91 functional by using the DMol^3 code [19]. The descriptions of the valence states have been obtained with the double numerical basis set augmented with polarization p-function (DNP), which has a computational precision being comparable with the Gaussian split-valence basis set 6-31G**. In this study, a (6, 6) graphene unit cell was used for all of the calculations. The Brillouin zone integration was carried out with 4 × 4 *k*-point sampling, where the convergence tolerance of the energy was set to 1.0×10^{-5} Ha and the maximum force was 0.002 Ha/Å. Transition states (TS) searches were performed using linear synchronous transit/quadratic synchronous transit (LST/QST) methods [20]. A refined reaction pathway constrained to the reactant, the presumed TS and the product has been obtained based on Nudged-Elastic Band (NEB) algorithm [21]. TS was confirmed by imaginary vibrational frequency.

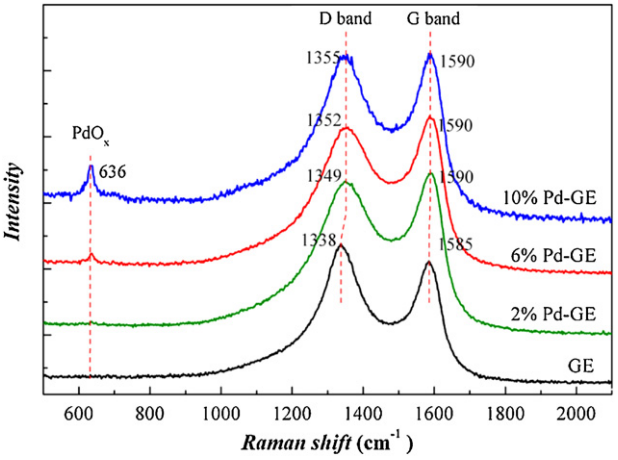

Fig. 2. Raman spectra of graphene and Pd-GE.

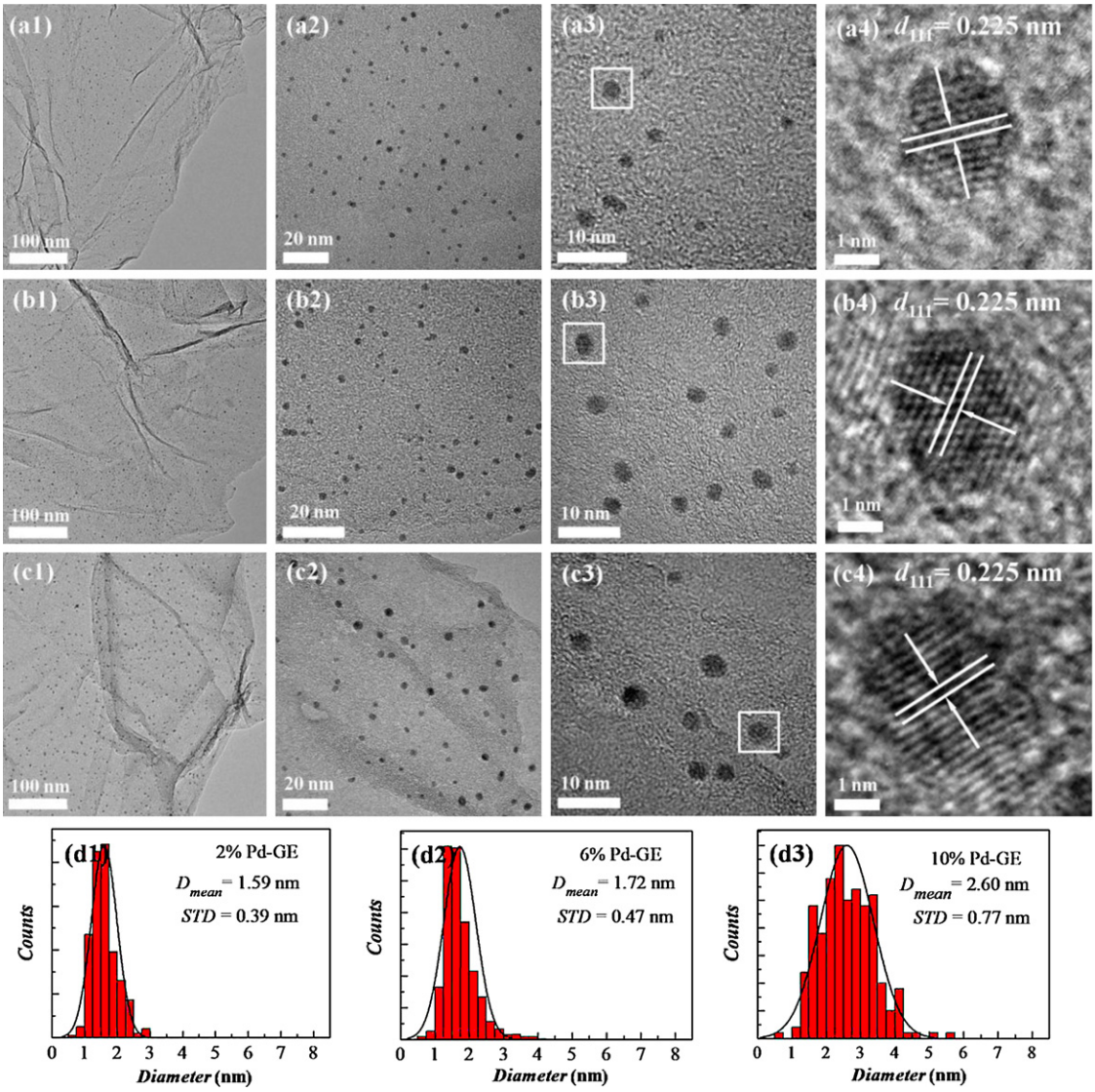

Fig. 3. TEM images of Pd-GE with different Pd loading 2% (a), 6% (b) and 10% (c), and the corresponding particle size distributions (d).

3. Results and discussion

3.1. Characterization of the catalysts

3.1.1. XRD characterization

Fig. 1 exhibits XRD patterns of the Pd-GE samples. The Pd peaks appear at 40.05°, 46.60°, 68.14° and 82.04°, which are attributed to the (1 1 1), (2 0 0), (2 2 0), and (3 1 1) planes of face-centered cubic structure of Pd (JCPDS no. 46-1043), respectively. Pd diffraction peaks are not clearly resolved in the case of 2% Pd-GE, and only weak peaks present for 6% Pd-GE, while they can be identified clearly for the 10% Pd-GE. The main Pd(1 1 1) peak in 10% Pd-GE suggests the crystal phase formed when the Pd loading is increased to 10%. The broad Pd peaks imply that highly dispersed Pd nano particles exist in the sample. Meanwhile, broad diffraction peaks at 25.10° for both graphene and Pd-GE samples exhibit carbon structure of graphene.

3.1.2. Raman spectra

Raman spectra clearly show the distinct graphene D-band and G-band for 2%, 6%, 10% Pd-GE composites. As illustrated in Fig. 2, the graphene sample shows a G band at 1585 cm^{-1}, a D band at 1338 cm^{-1} and a weak 2D band at 2685 cm^{-1} [22] (2D band is not shown here). After the Pd particles were embedded to the sample, the G band is blue shifted to 1590 cm^{-1} and the D band to 1349, 1352 and 1355 cm^{-1} for the 2%, 6% and 10% Pd-GE, respectively. The shift of G band is caused by the resonance of increased isolated double bonds at higher frequencies and the shift of D band is attributed to structural disorder at defect sites [7]. Moreover, an evident decrease of the I(D)/I(G) ratio is an indication of 'graphitization', which is caused by deprivation of parts of oxygen functionalities on the surface of graphene during the hydrogen reduction. In fact, there are many oxygen groups in the graphene sheets prepared by thermal exfoliation, which could be partly removed in a hydrogen atmosphere at the thermal reduction temperature. The left groups and defects may act as nucleating centre of the metal nano particles. Thus, it indicates that the graphene structures remain stable during the embedding of Pd nano particles. It can be also confirmed by Raman analyses that Pd nano particles have a strong interaction with the oxygen groups on the graphene by the appearance of the peak at 636 cm^{-1} [23].

3.1.3. TEM studies

The morphological structure, particle size, and metal dispersion of Pd-GE catalysts were further examined by TEM (Fig. 3). By the hydrogen reduction, the highly dispersed Pd nano

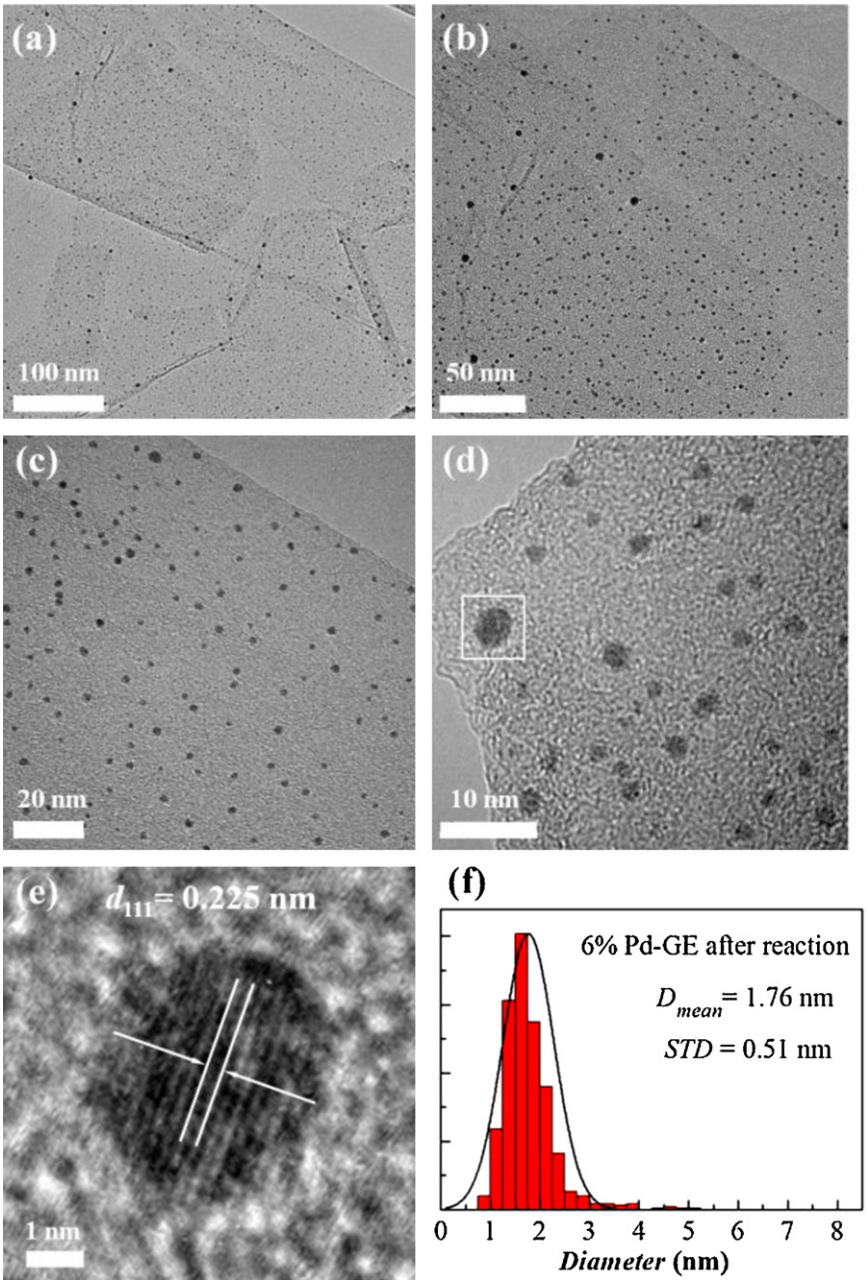

Fig. 4. TEM images of 6% Pd-GE after CO oxidation test.

particles were nucleated on the graphene surface. The high-resolution TEM images show well-defined lattice fringes of Pd(1 1 1), which indicates that the Pd nano particles are crystalline. The average diameters of the Pd nano particles and the standard deviation (STD) were obtained by analysing numerous TEM images like those depicted in Fig. 3. Pd nano particles are 1.59 ± 0.39 nm, 1.72 ± 0.47 nm and 2.60 ± 0.77 nm in diameter, corresponding to 2%, 6% and 10% Pd weight content in the Pd-GE catalysts, respectively. These results suggest that the Pd nano particles are uniformly embedded in the graphene and the size of the Pd nano particles can be tuned by varying the Pd loading amount. The growth of the Pd nano particles on the graphene is related to the oxygen functional groups on the surface. A strong interaction between the Pd atoms and the functional groups permits only the adjacent Pd atoms to combine together. Therefore the size of the Pd nano particles on the graphene is related to the density of the Pd ions on the graphene surface, which mainly depends on the Pd loading. Furthermore, TEM images in Fig. 4 of the catalyst (take 6% Pd-GE for example) after CO oxidation illustrate that the Pd particle size (1.76 ± 0.51 nm in diameter) does not change significantly in size during the reaction. Because of the active oxygen groups, some thin layers consisting of PdO_x may always exist or construct rapidly between the Pd nano particles and the graphene, which can firmly anchor Pd nano particles in the graphene. It also favors the stability of Pd-GE.

3.1.4. XPS analysis

It is reported in the literature that Pd catalysts for CO oxidation may exist in three forms (Pd^0 [15,24], PdO [25] and PdO_2 [26]). In Fig. 5b and d, the XPS spectra of Pd3d in 6% and 10% Pd-GE are depicted. These spectra can be fitted with three peaks associated with Pd in three different kinds of chemical states, a mainly Pd metal, while Pd(II) and Pd(IV) co-exist. And in Fig. 5a and c, C1s spectra are depicted which can be de-convoluted into five

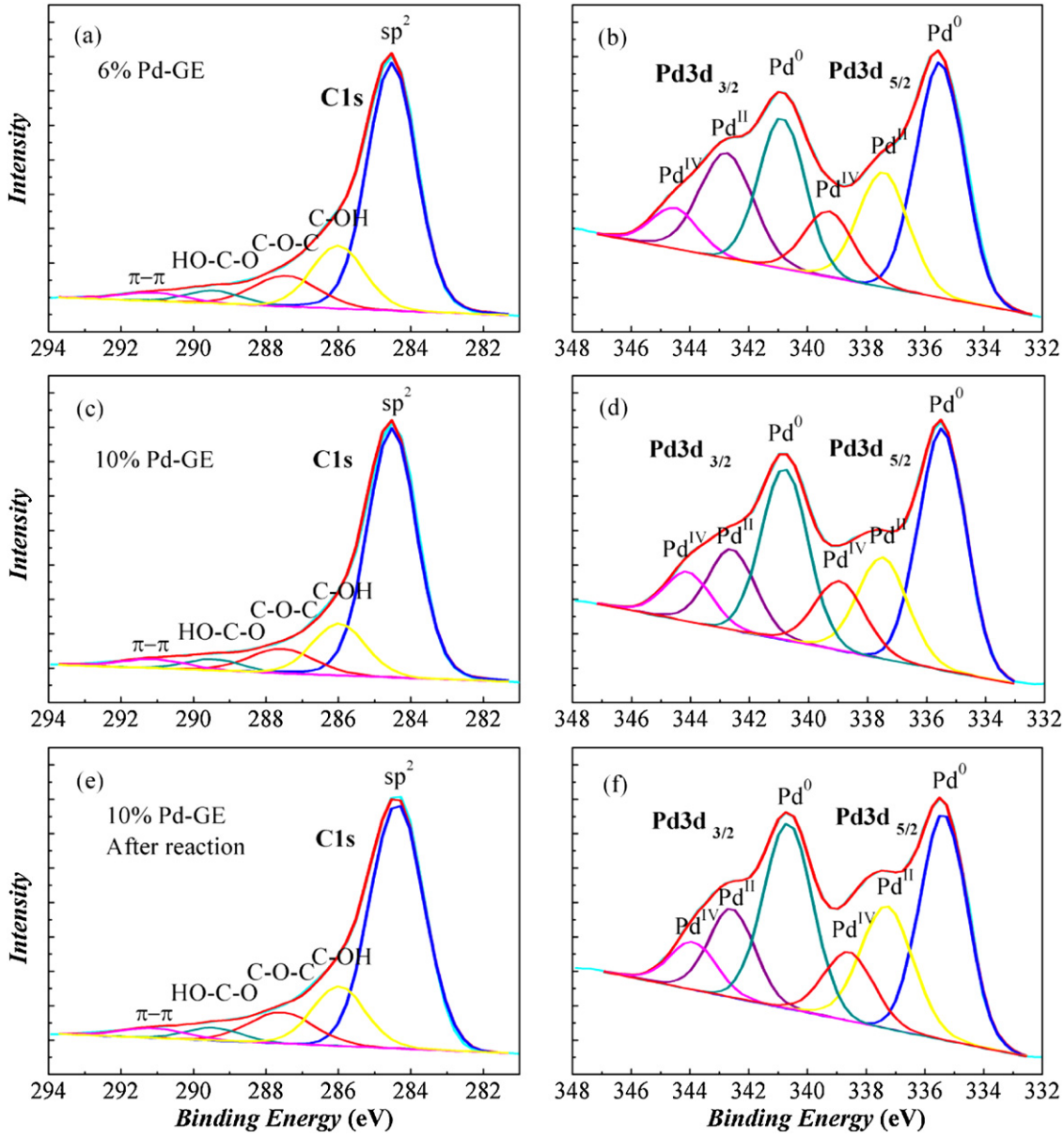

Fig. 5. XPS spectra of 6% (a, b) and 10% Pd-GE (c, d) before reaction, and 10% Pd-GE (e, f) after CO oxidation reaction.

peaks, ascribed to C—C, C—OH, C—O—C, HO—C=O and π–π^* bonds in graphene, respectively. The binding energies and area percentages of C1s and Pd3d in graphene and Pd-GE were analyzed in further detail in Table S1. It has been shown that part of carbonyl and other oxygen functional groups are removed during the hydrogen reduction at 300 °C, while the other oxygen groups remaining on the graphene may reconstruct with the Pd nano particles, leading to the formation of Pd(II) and Pd(IV). Nevertheless, we assume that as long as the Pd metal exists, the CO oxidation reaction occurs on the surface [27]. The effect of PdO_x towards CO oxidation is discussed in the supplementary data.

Besides, Fig. 5e and f demonstrate the XPS spectra of the 10% Pd-GE sample after the 10 h CO oxidation reaction. By comparison with the C1s spectra before the reaction, the ratio of the oxygen functional groups on graphene has almost no change after the reaction. Meanwhile, both the slight decrease of Pd^0 area and the increase of Pd(II) in the Pd3d spectra suggest that the metallic Pd on the particle surface are oxidized partially. We presume that a small quantity of dissociated oxygen can adsorb intensively on the Pd atoms when the reaction is discontinued by purging pure argon. However, most of the Pd atoms remain metallic. The related mechanism of CO oxidation will be discussed later.

3.1.5. DFT calculations

It is well known that the hydroxyl and epoxy are the major oxygen species on the graphene, which has been characterized by our experimental study. Stimulated from these experimental results, we investigated the adsorption of Pd adatoms on graphene with different surface properties, including pristine graphene, graphene with one hydroxyl group and graphene with one or two oxygen atoms in order to understand the role of oxygen species in stabilizing the Pd nano particles. The free energy diagrams for different systems as a functional of the oxygen chemical potential and the top view of geometry are shown in Fig. 6a and b. It is seen that the bridge of two neighboring carbon is the most favorable adsorption site of Pd on pristine graphene. Meanwhile, on graphene with one hydroxyl or oxygen, the favorable site of Pd is the atop of the neighboring carbon of oxygen species. On graphene with two oxygen, Pd is located on the bridge of two oxygen. And all of oxygen changes from the bridge to atop site after Pd adsorption.

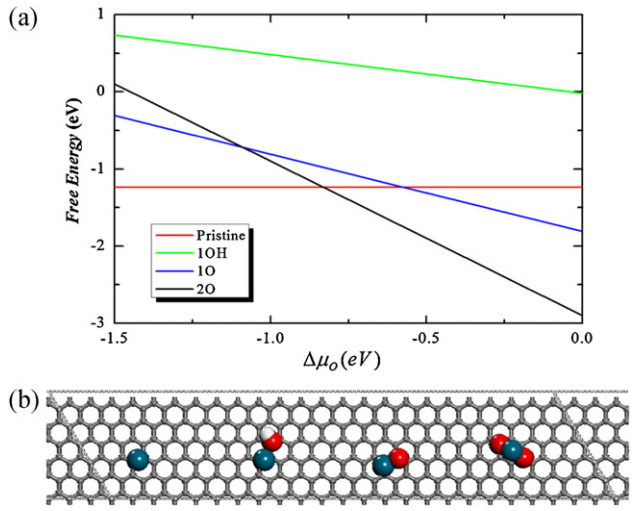

Fig. 6. (a) Free energy diagrams of Pd1/GE with different oxygen groups as a functional of oxygen chemical potential. The chemical potential of H_2O is chosen to −2.96 eV, corresponding to $p(H_2O) = 10^{-10}$ atm at 298.15 K; (b) top view of the geometric structures of Pd adsorbed on graphene.

Especially, oxygen species improve the adsorption of Pd adatoms on graphene. For example, the adsorption energy of Pd adatom on graphene with two oxygen is 2.3 times of that on the pristine one (Fig. S8a). From these diagrams (Fig. 6a), the most stable phase is Pd adatoms on the graphene with two oxygen when oxygen chemical potential is larger than −0.84 eV. Therefore, under our experimental conditions, the observed Pd nano particles should be adsorbed on graphene with oxygen-containing species.

Furthermore, we investigated the adsorption of a medium size Pd_7 clusters on the (6, 6) graphene with the four oxygen atoms. Two layer Pd_7 cluster is identified as the most stable adsorption configuration on the graphene. In the first layer, four Pd atoms are directly bonded with the oxygen. The average charge per Pd in the first and second layer is 0.20 and 0.01 based on Hirshfeld analysis, which is in good agreement with the XPS analysis. Combined with the experimental XPS, Raman and theoretical DFT results, it can be concluded that the Pd clusters tend to take on multilayer structure, with which the first layer mainly presents as PdO_x form and the dominant composite of other layers is Pd metal (Fig. 11b). Therefore, two layer Pd_7 cluster is a suitable model to investigate the reaction mechanism of CO oxidation.

3.2. The catalytic test on CO oxidation

3.2.1. Activity, stability and the kinetic studies

The Pd-GE catalysts were further tested with CO oxidation to determine catalytic activities. Fig. 7 shows the CO oxidation activity of the Pd-GE in the temperature range of 40–160 °C. Under the reaction conditions, the CO conversion increases gradually with the increasing temperature. Besides, a sharp increase can be observed when the temperature is close to T_{100} (100% CO conversion). T_{100} can be achieved at 144 °C, 127 °C and 119 °C, respectively, over catalysts with 2%, 6% and 10% Pd loading. Obviously, the higher Pd loading leads to the higher activity at the same temperature, while, the pure graphene support has no activity at all. In order to know the intrinsic activities of the Pd-GE catalysts, turnover frequencies (TOF) are normalized as the number of CO molecules reacting per active site per second. The dispersion D is estimated from the TEM mean particle diameters, assuming spherical particles [28]. The TOF values of Pd-GE at 100 °C and 110 °C are depicted in Fig. 8 and Table 1. It can be seen that the TOF also increase with the increasing of Pd loading.

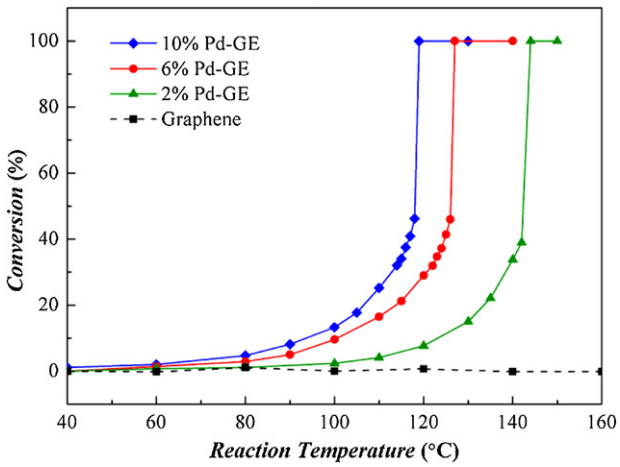

Fig. 7. Temperature dependence of the CO oxidation reaction for graphene and Pd-GE catalysts.

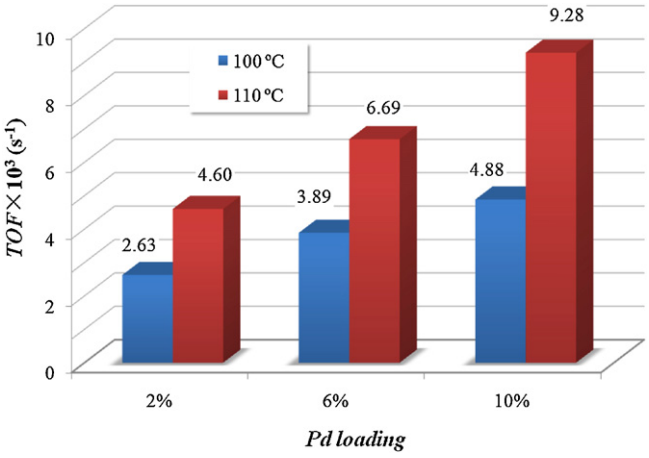

Fig. 8. TOF values at 100 °C and 110 °C for different Pd loading.

In addition, the catalytic activity of the Pd-GE is steady. For instance, 10% Pd-GE catalyst revealed good stability at the reaction temperature of 100 °C and 120 °C, which is shown in Fig. 9. The conversion of CO at 100 °C almost keeps steady around 10% throughout the 24 h reaction. Exactly, the conversion reaches 15% at the initial moment. However, after the reaction lasted for 1 h, it drops to 10%

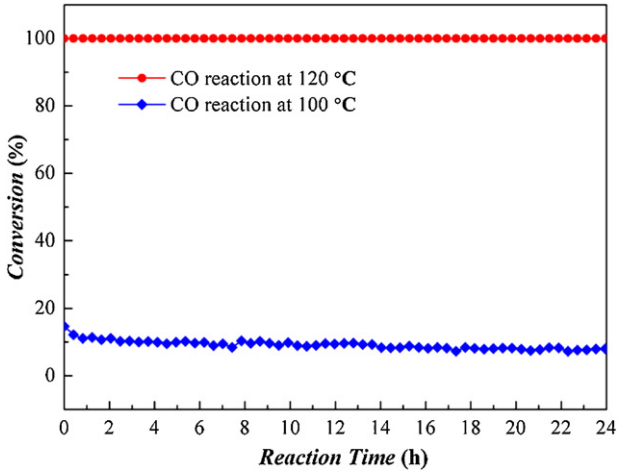

Fig. 9. The stability of 10% Pd-GE catalyst for CO oxidation at 100 °C and 120 °C.

Table 1
Pd nano particles size, metal dispersion, apparent activation energy, and TOF values at 100 °C and 110 °C for different Pd loadings.

Sample	Size/nm	Dispersion	E_a/kJ mol^{-1}	TOF$_{100\,°C}$ × 10^3 s^{-1}	TOF$_{110\,°C}$ × 10^3 s^{-1}
2% Pd-GE	1.59 ± 0.39	0.70	81.2 ± 3.5	2.63	4.60
6% Pd-GE	1.72 ± 0.47	0.65	66.0 ± 1.3	3.89	6.69
10% Pd-GE	2.60 ± 0.77	0.43	61.3 ± 2.6	4.88	9.28

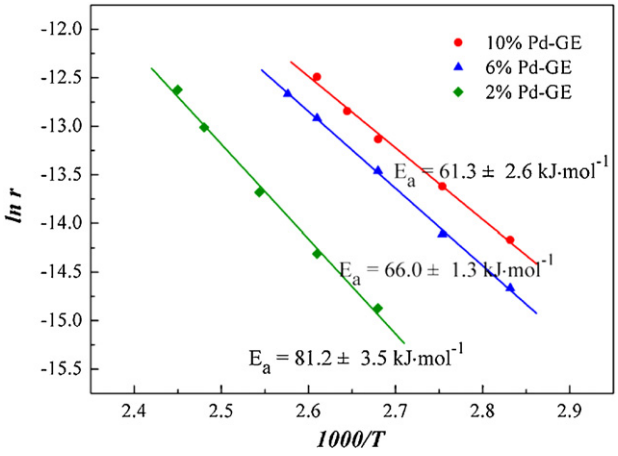

Fig. 10. Arrhenius plots for CO oxidation over Pd-GE catalysts.

more or less, and after 14 h, it becomes lower than 9.5% gently. On the other hand, the CO conversion at 120 °C could retain 100% during the testing time. The similar stability results can be found in other catalysts, such as Pd/SBA-15 [15] and Au/TiO_2 [29]. Considering the mechanism of the CO oxidation over our catalyst discussed later, it is suggested that at 100 °C the adsorbed CO have not occupied all of active sites on the Pd nano particles at the beginning. With the time going on, the chemisorption of CO is approaching to saturation, leading to the difficulty in the dissociation adsorption of O_2. At 120 °C, the energy is enough to dissociate the O_2 molecule, so that the reaction is always running smoothly during 24 h. This can also explain indirectly the previously mentioned sharp increase in CO conversion.

The Arrhenius plots are shown in Fig. 10, corresponding to the data in Fig. 7. From the slope of the plot, the apparent activation energy (E_a) can be estimated to be 81.2 kJ mol^{-1}, 66.0 kJ mol^{-1} and 61.3 kJ mol^{-1}, for the 2%, 6% and 10% Pd-GE catalysts, respectively. This is basically consistent with the other Pd supported catalysts in the literature [30,31]. Importantly, the E_a values of the three catalysts are different from each other, which could be in favor of the TOF values. Additionally, the reaction order shown in Fig. S9 was measured at 100 °C over the 10% Pd-GE catalyst through the regulation of the CO or O_2 partial pressure. In this condition, the reaction order of CO and O_2 are −0.64 and 1.45, respectively. Based on the E_a values and the reaction order [31–33], we propose the CO oxidation should be accomplished mainly via the L–H mechanism, where the chemisorbed CO reacts with the chemisorbed oxygen. This conclusion will be confirmed by the following DFT studies.

3.2.2. DFT studies on the mechanism

In order to further provide the insight of reaction mechanism of CO oxidation on Pd-GE catalyst, Fig. 11a shows the potential energy diagram of CO oxidation on Pd_7 cluster supported on graphene. After the co-adsorption of CO and O_2, the first elementary step is the dissociation of the adsorbed O_2, which is exothermic by 0.32 eV. The transition state configuration of O_2 dissociation is shown in Fig. 11c, in which the distance of oxygen–oxygen is 2.30 Å. The reaction barrier of the first elementary step is 0.67 eV. After that, one of the O

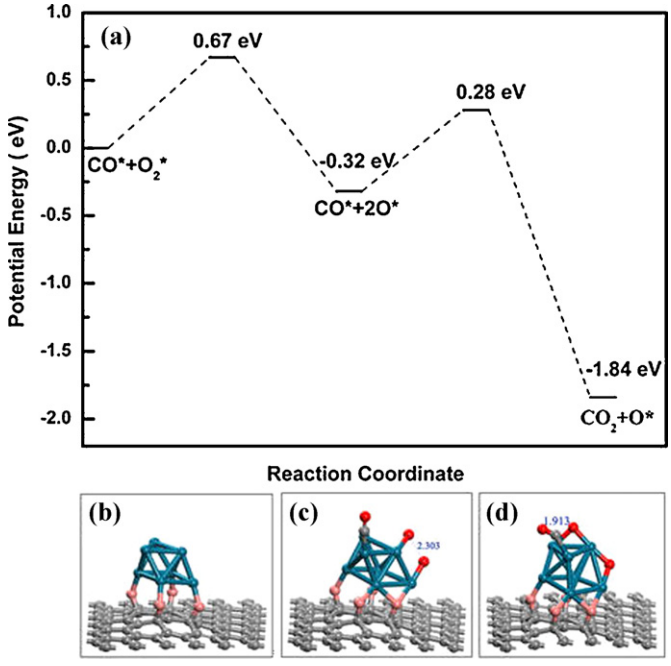

Fig. 11. (a) Potential energy diagrams for CO oxidation over Pd-GE catalyst corresponding to the local configurations; (b) two layer Pd_7 cluster adsorbed on the graphene; (c, d) transition states for the CO oxidation.

atoms bound with Pd reacts with an adsorbed CO molecule. For this process, it is exothermic by 1.84 eV, with an energy barrier of 0.60 eV. The produced CO_2 molecule is easy to be desorbed due to the much lower adsorption energy (shown in Fig. 11d). A microkinetic model with five elementary steps is proposed (Part IV in the supplement). The reaction order, the calculated rate constant and activation energy based on DFT calculations are all in well agreement with these obtained from experimental studies. Therefore, we can conclude that the CO oxidation over the Pd-GE catalysts follows the L–H mechanism.

4. Conclusion

In summary, graphene supported Pd catalyst has been synthesized by the conventional impregnation and hydrogen reduction. The Raman and XPS characterization show the existence of oxygen containing groups even after hydrogen reduction. Based on DFT total energy calculations and thermodynamic analyses, the Pd nano particles is stable on the graphene sheets with oxygen groups. Therefore, our study reveals that the oxygen containing groups play a vital role in stabilizing Pd clusters on graphene. The Pd-GE catalyst shows superior activity and stability for CO oxidation. The kinetic studies from both experimental and DFT calculations indicate that CO oxidation on this system follows the Langmuir–Hinshelwood (L–H) mechanism. The present study is helpful for the design of graphene supported noble metal catalysts with high activity and stability for gaseous reactions.

Acknowledgements

The financial support from the National Natural Science Foundation of China (#20990223 and 21176221) and 111 project of Ministry of Education of China is greatly appreciated.

Appendix A. Supplementary data

Supplementary data associated with this article can be found, in the online version, at http://dx.doi.org/10.1016/j.apcatb.2012.05.023.

References

[1] C.J. Liu, U. Burghaus, F. Besenbacher, Z.L. Wang, ACS Nano 4 (2010) 5517–5526.
[2] Y.F. Li, Z. Zhou, G.T. Yu, W. Chen, Z.F. Chen, Journal of Physical Chemistry C 114 (2010) 6250–6254.
[3] T.G. Xu, L.W. Zhang, H.Y. Cheng, Y.F. Zhu, Applied Catalysis B: Environmental 101 (2011) 382–387.
[4] Y.J. Wang, R. Shi, J. Lin, Y.F. Zhu, Applied Catalysis B: Environmental 100 (2011) 179–183.
[5] Y. Wang, C.X. Guo, X. Wang, C. Guan, H.B. Yang, K.A. Wang, C.M. Li, Energy & Environmental Science 4 (2011) 195–200.
[6] H. Li, S. Pang, X. Feng, K. Mullen, C. Bubeck, Chemical Communications 46 (2010) 6243–6245.
[7] A.R. Siamaki, A.E.R. Khder, V. Abdelsayed, M.S. El-Shall, B.F. Gupton, Journal of Catalysis 279 (2011) 1–11.
[8] S. Sharma, A. Ganguly, P. Papakonstantinou, X.P. Miao, M.X. Li, J.L. Hutchison, M. Delichatsios, S. Ukleja, Journal of Physical Chemistry C 114 (2010) 19459–19466.
[9] N. Farhangi, R.R. Chowdhury, Y. Medina-Gonzalez, M.B. Ray, P.A. Charpentier, Applied Catalysis B: Environmental 110 (2011) 25–32.
[10] S. Moussa, A.R. Siamaki, B.F. Gupton, M.S. El-Shall, ACS Catalysis 2 (2012) 145–154.
[11] Y.J. Hu, P. Wu, Y.J. Yin, H. Zhang, C.X. Cai, Applied Catalysis B: Environmental 111 (2012) 208–217.
[12] S. Moussa, V. Abdelsayed, S. El-Shall M, Chemical Physics Letters 510 (2011) 179–184.
[13] Q. Ge, S.J. Jenkins, D.A. King, Chemical Physics Letters 327 (2000) 125–130.
[14] E. Kadossov, U. Burghaus, Catalysis Letters 134 (2010) 228–232.
[15] H.P. Wang, C.J. Liu, Applied Catalysis B: Environmental 106 (2011) 672–680.
[16] S. Paul, E.E. Santiso, M.B. Nardelli, Journal of Physics: Condensed Matter 21 (2009) 355008.
[17] W. Hummers, R. Offeman, Journal of American Chemical Society 80 (1958) 1339.
[18] H.C. Schniepp, J.L. Li, M.J. McAllister, H. Sai, M. Herrera-Alonso, D.H. Adamson, R.K. Prud'homme, R. Car, D.A. Saville, I.A. Aksay, Journal of Physical Chemistry B 110 (2006) 8535–8539.
[19] B. Delley, The Journal of Chemical Physics 92 (1990) 508–517.
[20] N. Govind, M. Petersen, G. Fitzgerald, D. King-Smith, J. Andzelm, Computation Materials Science 28 (2003) 250–258.
[21] S.A. Trygubenko, D.J. Wales, The Journal of Chemical Physics 120 (2004) 2082–2094.
[22] J.L. Dattatray, U. Maitra, L.S. Panchakarla, U.V. Waghmare, C.N.R. Rao, Journal of Physics: Condensed Matter 23 (2011) 055303.
[23] M.A. Castro, A.J. Aller, A. McCabe, W.E. Smith, D. Littlejohn, Journal of Analytical Atomic Spectrometry 22 (2007) 310–317.
[24] A.S. Ivanova, E.M. Slavinskaya, R.V. Gulyaev, V.I. Zaikovskii, O.A. Stonkus, I.G. Danilova, L.M. Plyasova, I.A. Polukhina, A.I. Boronin, Applied Catalysis B: Environmental 97 (2010) 57–71.
[25] S.H. Oh, G.B. Hoflund, Journal of Catalysis 245 (2007) 35–44.
[26] J.Y. Ye, C.J. Liu, Chemical Communications 47 (2011) 2167–2169.
[27] K. Zorn, S. Giorgio, E. Halwax, C.R. Henry, H. Grönbeck, G. Rupprechter, Journal of Physical Chemistry C 115 (2010) 1103–1111.
[28] C. Mohr, H. Hofmeister, P. Claus, Journal of Catalysis 213 (2003) 86–94.
[29] B. Schumacher, V. Plzak, M. Kinne, R.J. Behm, Catalysis Letters 89 (2003) 109–114.
[30] L. Liu, F. Zhou, L. Wang, X. Qi, F. Shi, Y. Deng, Journal of Catalysis 274 (2010) 1–10.
[31] J. Szanyi, D.W. Goodman, Journal of Physical Chemistry 98 (1994) 2972–2977.
[32] T. Matsushima, D.B. Almy, D.C. Foyt, J.S. Close, J.M. White, Journal of Catalysis 39 (1975) 277–285.
[33] F. Gao, Y. Wang, Y. Cai, D.W. Goodman, Journal of Physical Chemistry C 113 (2008) 174–181.